Calcif Tissue Int (1993) 53:249–256

Calcified
Tissue
International
© 1993 Springer-Verlag New York Inc.

Laboratory Investigations

Epitaxial Overgrowth of Apatite Crystals on the Thin-Ribbon Precursor at Early Stages of Porcine Enamel Mineralization

Y. Miake,[1] S. Shimoda,[2] M. Fukae,[2] and T. Aoba[3]

[1]Tokyo Dental College, Masago, Chiba, Japan; [2]Tsurumi University School of Dentistry, Yokohama 230, Japan; and [3]Forsyth Dental Center, 140 Fenway, Boston, Massachusetts 02115, USA

Received February 15, 1993, and in revised form April 5, 1993

Summary. The aim of the present work was to investigate changes in cross-sectional morphologies of enamel crystallites as a function of location in secretory porcine enamel. Enamel tissues were obtained from 5- to 6-month-old slaughtered piglets. For examination by electron microscopy, a portion of the secretory enamel was embedded in resin and ultrathin sections were prepared with a diamond knife. In parallel studies, compositional and structural changes of enamel mineral were assessed by chemical analysis and Fourier transform infrared (FTIR) spectroscopy. For this purpose, two consecutive layers of the outer secretory enamel, each approximately 30 μm thick, were separated from the labial side of permanent incisors. Using high-resolution electron microscopy, early events of enamel crystal growth were characterized as the epitaxial growth of small apatite units on the lateral surfaces of the initially precipitated thin ribbon. These apatite units had regular triangle or trapezoid cross-sections. After fusions of those isolated trapezoids on both lateral sides of the platy template, the resulting enamel crystallites had the well-documented flattened-hexagonal shapes in cross-sections. The initially precipitated thin plate was buried inside the overgrown apatite lamella and then retained as a central dark line. Similar morphological evidence for the epitaxial nucleation and overgrowth of carbonatoapatite on the platy template was obtained *in vitro*. Chemical and FTIR analyses of the enamel layer samples showed that the characteristics of the youngest enamel mineral were distinct from those of enamel crystals found in older secretory enamel. The overall results support the concept that initial enamel mineralization comprises two events: the initial precipitation of thin ribbons and the subsequent epitaxial growth of apatite crystals on the two-dimensional octacalcium phosphate–like precursor.

Key words: Enamel – Amelogenesis – Crystal growth – Calcium phosphates – Biomineralization.

In the mineralization process taking place in early stages of mammalian amelogenesis, the morphology of the initially formed crystals is thin ribbons and their subsequent growth gives rise to elongated plates having flattened hexagonal cross-sections [1–3]. Much interest has been directed to the fact that the thin-ribbon morphology is more consistent with the morphology of octacalcium phosphate (OCP) crystallites than it is with the hexagonal symmetry of apatite crystals [4, 5]. However, the existence of OCP has not been demonstrated in developing enamel tissues. Moreover, details of the growth process of enamel crystals still remain elusive. Particularly, there is a paucity of information as to how the cross-sectional morphology of enamel crystallites changes from the original plate of one- or two-unit cells wide to the flattened hexagonal shape. Other unresolved questions are whether the size and shape of enamel crystallites are primarily controlled by physico-chemical mechanisms, and what is the role of the secreted matrix proteins in the initial stage of enamel mineralization.

Recent *in vitro* studies [6–8], using high-resolution electron microscopy, clearly demonstrated that apatite structures grow epitaxially on the (100) plane of OCP, thereby embedding the OCP lamella in the center of the apatite crystals. From this evidence, obtained in the absence of organic matter, it was inferred that similar physicochemical reactions may occur *in vivo*, giving rise to the characteristic morphology of enamel crystals. No direct evidence has been reported for the assumed epitaxial growth of apatite nuclei on OCP-like thin ribbons in the initial stage of enamel mineralization. Thus, using high-resolution electron microscopy, we attempted to visualize the precipitation and growth events taking place during the secretory stage of porcine amelogenesis. The rationales for use of this animal model are that (1) the chemical, biochemical, and ultrastructural aspects of early mineralization processes were delineated in our previous studies [9–12]; (2) the enamel prism structure is close to that of human enamel and less complex than that of bovine enamel; and (3) its wide secretory enamel provides the most convenient experimental system for investigation of morphological alterations of enamel crystallites progressively as a function of location from the outermost (youngest) secretory enamel toward the inner (older) secretory enamel. Moreover, the pig enamel model allows us to collect sufficient amounts of young secretory enamel samples [9, 12]. Efforts were also taken, using chemical analysis and Fourier transform infrared spectroscopy (FTIR), to assess changes in the composition and structure of enamel mineral which are presumed to be in accord with morphological alterations of enamel crystallites.

Materials and Methods

Preparation of Secretory Porcine Enamel

Tooth germs of upper and lower permanent incisors were obtained

Offprint requests to: T. Aoba

from 5- to 6-month-old slaughtered piglets. The enamel organ was dissected out of the bones and then the covering soft tissues were removed. Prior to ultrastructural observations, the teeth obtained from the same animal were divided into two groups: (1) a group fixed with 2.5% glutaraldehyde-2.0% paraformaldehyde in 0.05 M cacodylate buffer and then dehydrated in a graded ethanol series; and (2) a group lyophilized without fixation and then immersed in absolute ethanol. All dehydrated specimens were embedded in Polyester resin (Rigolac-2004, Nissin EM Co., Tokyo). Portions of the embedded enamel within the zone of secretion were sliced transversely and then ground to yield thin sections of 0.5–1 mm thick. From those sections, three enamel zones (the outer, middle, and inner secretory enamel) were cut with a sharp razor blade. Each of the cut enamel specimens was re-embedded with POLY/BED 812, and ultrathin sections were prepared on a Sorvall Porter-Blum microtome equipped with a diamond knife. Water used for collecting the sections was presaturated with synthetic hydroxyapatite. The sections prepared from each resin block were transfered on holey carbon support films. Special care was given (1) to section enamel prisms perpendicular to their long axis, consequently making it possible to observe cross-sections of enamel crystallites; and (2) in cases of the outer enamel specimens, to prepare and collect ultrathin serial sections in order to examine progressive changes in crystal morphology taking place in the outer secretory zone close to the ameloblasts.

For chemical and FTIR analyses, the secretory enamel was collected from the labial side of the permanent incisors of age-matched animals. After removing the covering soft tissues, the exposed enamel surface was wiped gently with a paper tissue to remove the cellular debris and traces of blood. The outermost (youngest) secretory sample (here referred to as S1), less than 30-μm thick, was separated with a sharp razor blade. Subsequently, the second layer (S2), having about a 30-μm thickness, was obtained in the same way. Thicknesses of those separated enamel tissues were examined under a stereo-zoom microscope. Following removal of the two outer layers, the underlying inner secretory enamel (S3) was scrapped as a whole with a small spatula. In order to collect sufficient amounts of S1 and S2 samples, dissection of the secretory enamel was conducted on 50 or more teeth. The enamel samples corresponding to each zone were pooled. Each of the pooled enamel samples was lyophilized and then stored at −30°C until used for analyses.

Synthetic Carbonatoapatites. For comparative purposes, the morphology of carbonatoapatites precipitated in aqueous media was examined by electron microscopy. The precipitation reaction was started by simultaneously delivering calcium and phosphate solutions into a reaction solution that was adjusted to 80 ± °C and neutral pH (7.2–7.4). Details of the experimental conditions and procedures have been previously reported [13]. When precipitates appeared in the reaction solution, an aliquot of the suspension was withdrawn. The solid in the suspension was separated quickly by centrifugation at 4°C, washed with ice-cold deionized water, and then lyophilized. For observation of the recovered crystals at low magnifications, the powder sample was suspended in absolute ethanol and then transferred onto microgrids supported with carbon films. For the high-resolution studies, the solid was embedded in POLY/BED 812 resin, and ultrathin sections were prepared in the same way as described for enamel specimens.

Electron Microscopy. The cross-sectional morphology of enamel and synthetic crystals was observed, without staining, at direct magnifications of 50–100 K in a JEM 1200EX electron microscope at 120 kV. High-resolution lattice fringes were obtained at a direct magnification of 300 K, using JEM-2000FX II and 2010 electron microscopes at 200 kV. To minimize electron beam-damage to the crystallites, a specimen holder was cooled with liquid nitrogen, and electron currencies were kept at the lowest levels. Furthermore, crystallites showing desirable orientations were searched on a video camera-image enhancing system attached to the electron microscope.

Chemical Analyses of Enamel Samples

In order to gain information on the possibility of OCP precipitation in enamel mineralization, the acid phosphate content of the dissected enamel samples was determined according to the procedure of Gee and Dietz [14]. Each of the pooled powder enamel samples were plasma ashed at about 60°C (to remove organic matter and carbonate on crystal surfaces, which may interfere with pyrophosphate formation [12]) and then heated at 400°C for 12 hours. The pyrolysis conditions were chosen after a series of preliminary determinations to secure the maximum yield of pyrophosphate. We also determined the Ca, P, and CO_3 contents of the enamel samples. The Ca and P contents were determined by atomic absorption spectrophotometry and colorimetry, respectively. The CO_3 content of the enamel samples was determined by Conway's microdiffusion method [15] with $CaCO_3$ as standards. The estimated uncertainties for HPO_4, Ca, P, and CO_3 determinations were 6%, 4%, 1.5%, and 8%, respectively, of the analyzed quantities.

Fourier Transform Spectroscopy. FTIR spectra of the secretory enamel samples were recorded with a diffuse-reflectance attachment in a Perkin-Elmer 1640 FTIR. Each sample (about 1 mg) was mixed with KBr in an agate mortar. Sixty-four spectral scans were conducted over the wavenumber range of 4500–450 cm^{-1} with 4 cm^{-1} resolution. The number of bands and their locations were determined by taking the second derivative of the spectrum. As the secretory enamel was abundant in organic matter, spectral signals of the formed mineral crystals were overlapped with the signals originating from organic matter. Thus, difference spectra were obtained by subtraction between the experimental spectra recorded from the enamel sample and the organic matrix sample extracted from the outer secretory enamel. Preparation of the protein sample and its characterization were reported previously [16]. The second derivative and subtraction were obtained using software provided by Perkin-Elmer.

Results

Figure 1A–D shows typical low-magnification electron micrographs of porcine enamel crystallites, which were taken at various sites from the surface region toward the inner secretory enamel. In preliminary examination, it was confirmed that there were no marked variations in crystal morphology due to the different methods of processing the enamel specimens (i.e., fixation/dehydration versus lyophilization). Thus, micrographs shown here were taken from the fixed and then dehydrated samples unless otherwise specified. As previously documented [1–3], the youngest crystallites, which were found in a narrow zone adjacent to the secretory ameloblasts, were thin ribbons or needle-like in cross-sections (Fig. 1A). When observations were made on the serial sections corresponding to the outer enamel region, it was noticed that the contour of needles became irregular as a function of distance from the enamel surface. As indicated by arrows in Figure 1B, many dot-like structures or projections were discerned surrounding the needles. From the middle and inner regions as shown in Figures 1C and D, respectively, enamel crystallites having elongated hexagonal shapes in cross-sections were observed. Their thickness increased gradually and their contour became well faceted with advancement of mineralization. Most of the sectioned crystallites retained dark contrast in their central portion (central dark line). It should be noted that the thicknesses of the corresponding apatite crystallites were relatively uniform at certain sites, and that their lateral surfaces were relatively smooth and flat without distinctive projections. With the decrease in the intercrystalline space, due to partial degradation and removal of organic matter [9], some crystals were in contact with neighboring crystals or represented crystal branches. Those features may have been induced by fusions or lateral growing, as suggested by Daculsi et al. [17].

Figure 2 shows high-resolution electron micrographs of

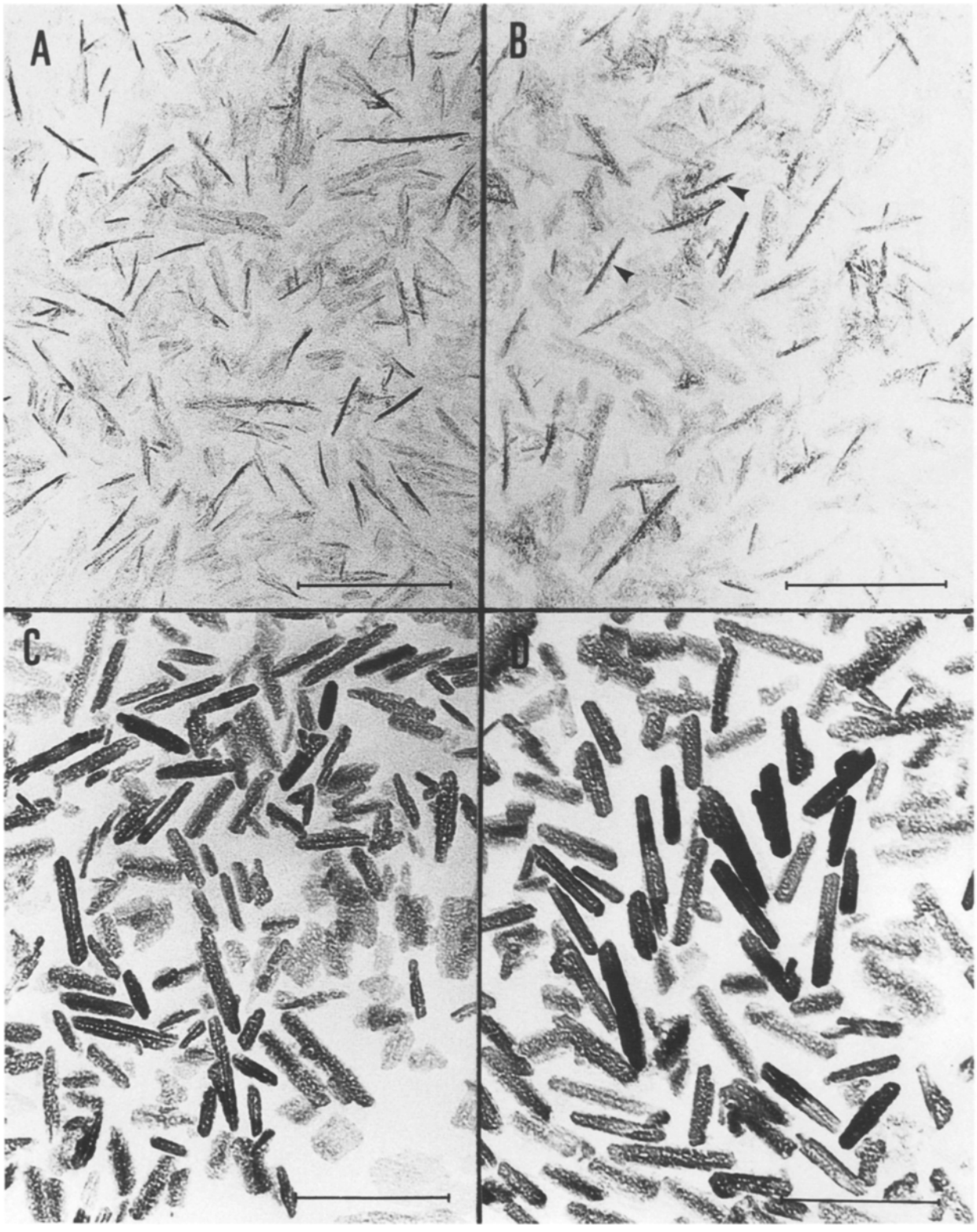

Fig. 1. Low magnification electron micrographs of secretory porcine enamel. **(A)** Thin ribbons, or needles in their cross-sections, found in the outermost zone in the vicinity of ameloblasts. **(B)** Crystals found in the outer secretory enamel slightly underlying from (A). Arrowheads indicate dot-like structures or projections surrounding the needles. **(C and D)** Crystals found in the middle and inner secretory enamel, respectively, had elongated hexagonal shapes in cross-sections. Horizontal bar corresponds to 100 nm.

enamel crystallites located at various sites within the secretory enamel. The youngest thin ribbon crystallites were as small as one- or two-unit cells wide (Fig. 2A). Their lateral surfaces remained relatively smooth and flat at the very beginning of precipitation. The following step of porcine enamel mineralization was characterized by the appearance of small, regular triangle and trapezoid crystal units on the surface of the thin ribbons (Fig. 2B,C). The intersecting lat-

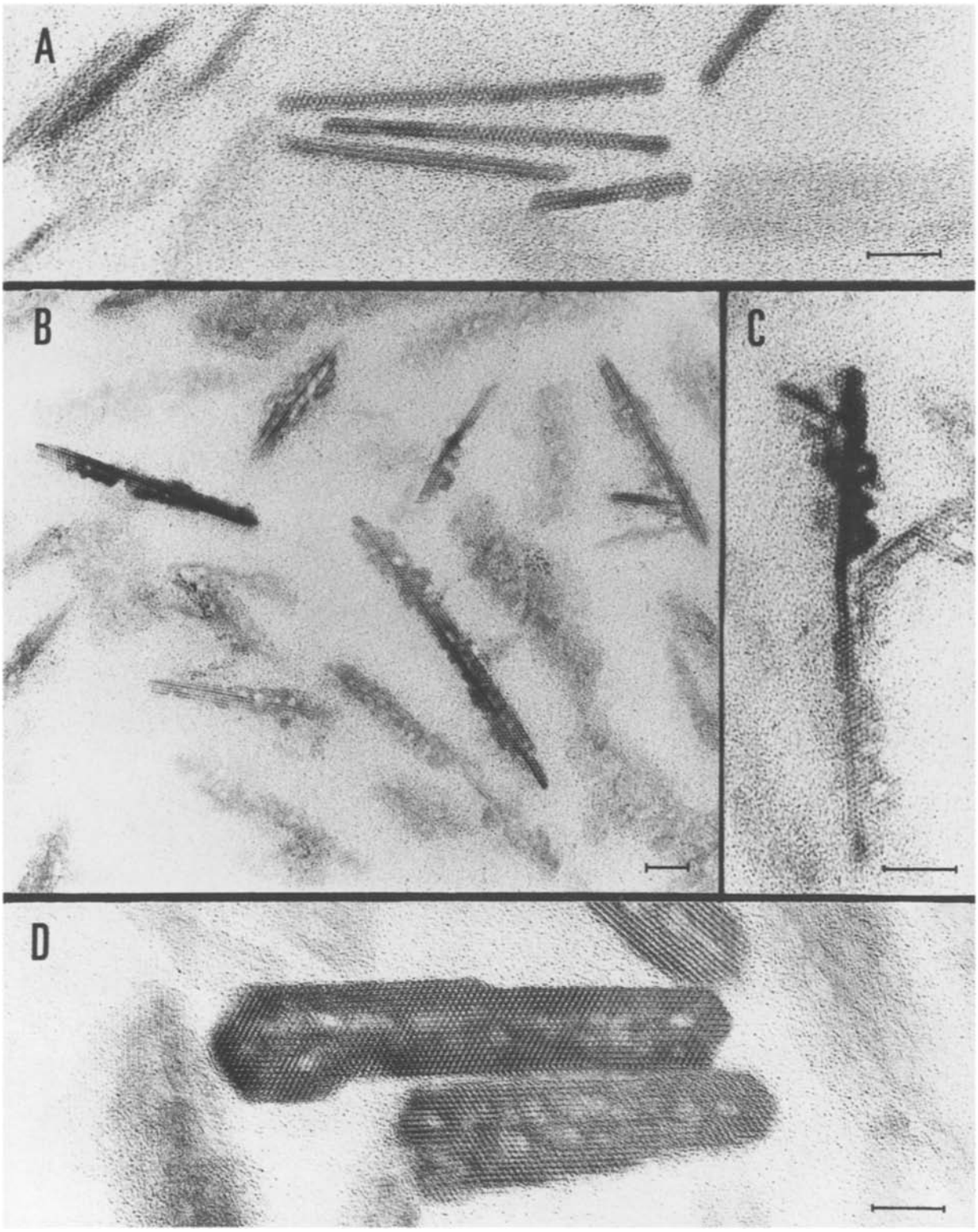

Fig. 2. High-resolution electron micrographs of porcine enamel crystals representing various steps of their crystal growth. **(A)** Cross-sectional images of thin ribbons precipitated in the outermost zone adjacent to the ameloblasts. **(B and C)** Non-uniform deposition of apatitic units on the lateral surfaces of thin ribbons. The corresponding micrographs were taken at sites that were slightly inward (10–20 μm in depth) from the outermost zone shown in (A). **(D)** Enamel apatite crystallites having well-faceted, characteristic flattened, hexagonal cross-sections, which were found in the middle-inner secretory enamel. Horizontal bar corresponds to 10 nm.

tice fringes found in each unit had an angle of 120°, which corresponds to the [0001] zone image of apatite crystals. Hohling et al. [18] reported the precipitation of dot-like isolated crystals, which appeared to be aligning linearly. In the present studies, careful examination of many serial sections at high magnifications showed that the dot-like structures at low magnifications (see Fig. 1B) corresponded to the small apatite units attached to the thin plate. Most likely, the reg-

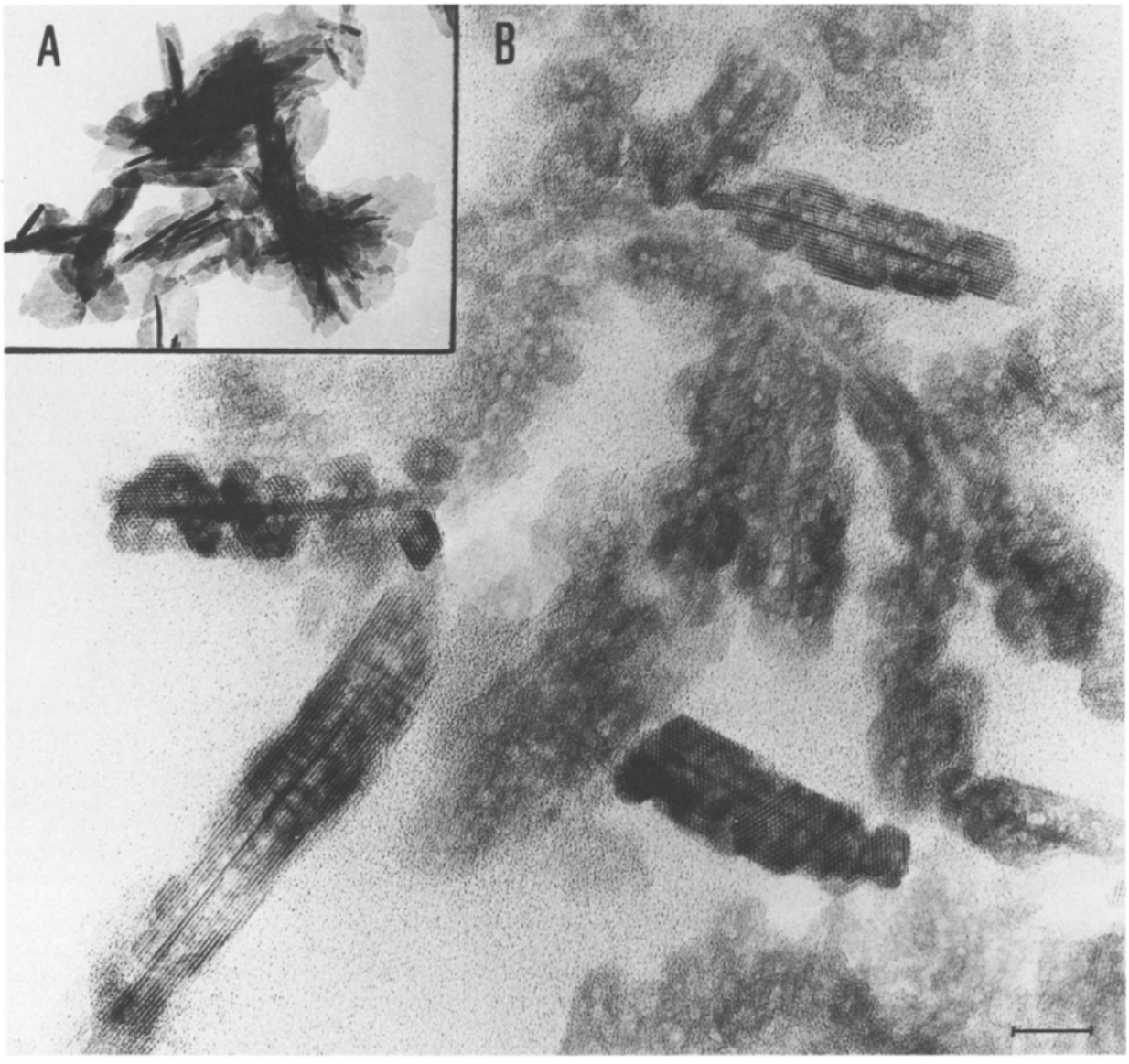

Fig. 3. Electron micrographs of synthetic carbonatoapatite. **(A)** Low-magnification micrograph showing thin plates in morphology. **(B)** High-resolution micrograph of their cross-sections, representing the sequential events of nucleation, overgrowth, and fusions of apatitic units on the plane having the dark contrast. The central dark line was retained in the apatite crystals after fusions of the overgrown units. Horizontal bar corresponds to 10 nm.

ular triangles represented the initial shape of apatite nuclei formed on the thin ribbon template and, with their growth in both horizontal and vertical directions, their cross-sectional morphology changed into trapezoids (see Discussion). It appears that the originally isolated trapezoids fused to each other on both sides of the thin plate, giving rise to elongated hexagonal shapes. Figure 2D shows the resulting enamel apatite crystallites having flattened hexagonal shapes, which were found in the middle to inner zones. Most of those crystallites retained defects in the central portion and steps of a few unit cells high on their lateral surfaces.

Figure 3 shows electron micrographs of synthetic carbonatoapatites. The precipitated crystals were characterized as thin plates (Fig. 3A), which had the composition of Ca 35.0 wt%, P 17.9 wt%, CO_3 2 wt%, and HPO_4 15% of the total P. Extensive surveys of sectioned crystallites at high magnifications disclosed that a small number of those crystallites retained a central dark line. This observation is in good agreement with the results reported by Nelson et al. [19]. As can be seen from Figure 3B, observations of more importance were that the epitaxial growth of apatite on the lateral planes of the thin platy precursor were reproduced *in vitro* and that the overgrowing apatite units displayed regular triangular and trapezoid shapes in cross-sections, resembling those found on enamel thin ribbons.

Table 1 gives chemical analyses of the dissected and pooled enamel samples. The outermost (youngest) secretory enamel (S1), which comprised mixtures of thin ribbons and overgrowing apatitic units, contained the highest HPO_4^{2-}, corresponding to about 22% of the total phosphate. With the increase in both Ca and P contents (i.e., advancement of enamel mineralization), the acid phosphate content decreased markedly from 15% of the total phosphate in S2 to 11% in S3. The steep decline of the acid phosphate content as a function of location within secretory porcine enamel is in good agreement with the results reported by Siew et al.

Table 1. Chemical composition of secretory porcine enamel

Sample	Depth (μm)	HPO_4 (% of total P)	Ca (wt%)	P (wt%)	CO_3 (wt%)
S1	30>	21.9 (0.2)	13.0 (0.03)	6.7 (0.02)	1.6 (0.3)
S2	30–60	15.2 (0.6)	19.6 (0.06)	10.0 (0.03)	2.5 (0.1)
S3	60<	11.7 (0.5)	24.2 (0.14)	12.3 (0.05)	3.2 (0.1)

S1, outermost secretory enamel; S2, outer secretory enamel; S3, inner secretory enamel. The analytical results are represented by the average (SE) of three determinations

[20], which were achieved using the rat incisor enamel model.

FTIR experimental spectra of the pooled enamel samples were characterized by the presence of a broad band of water around 3000 cm^{-1} and amide bands (the peak maxima for amide I, II, and III appeared at approximately 1660, 1515, and 1240 cm^{-1}, respectively) (Fig. 4, left side). A unique feature in the FTIR spectrum of the S1 enamel sample was the prominence of a PO_4 band at 1120 cm^{-1}; the corresponding band was assigned as originating from labile, nonapatitic pools of phosphate ions [21]. The PO_4 band at 1118 cm^{-1} already disappeared in the spectrum recorded from S2, supporting the fact that a rapid change in the properties of enamel mineral occurred within the narrow surface zone. The spectra of both S2 and S3 samples were characterized by the prominent CO_3 bands in the range of 1560–1420 and 880–870 cm^{-1}. As shown in the last column of Table 1, chemical analysis confirmed that the S2 and S3 enamel samples contained significant amounts of carbonate. From difference spectra shown in the right side of Figure 4, it was verified that, in addition to the changes of the PO_4 band at 1118 cm^{-1}, the peak maxima of the PO_4 band was shifted gradually from 1026 cm^{-1} for S1 to 1030 cm^{-1} for S2 and 1035 cm^{-1} for S3. The observed shifts of the PO_4 peak maxima may be interpreted either by mineral maturation from OCP-like precursors into apatitic crystals [22], or by improvement of apatite crystallite perfection, as reported by Pleshko et al. [23].

Discussion

The nucleation and overgrowth of apatitic units on enamel thin ribbons are considered to represent the same phenomenon as the *in vitro* apatite formation on OCP template, which was most elegantly demonstrated by Iijima et al. [7, 8]. As we reported previously [24], the *in vivo* morphological evidence for the apatite overgrowth on thin plates was obtained from developing fish enameloid, which contained relatively low fluoride. The current HPO_4 and FTIR analyses showed that the characteristics of the youngest enamel mineral are distinct from those of enamel crystals found in older secretory enamel. The high acid phosphate content of the youngest enamel might be interpreted as indicative of the formation of OCP at the very beginning of amelogenesis. However, it should be noted that it is very difficult to obtain indisputable evidence for the existence of OCP (such as one-unit cell intergrowth) in those biosystems. Indeed, the decrease of the HPO_4 content and the peak shifts of PO_4 bands with age also might be explained by changes in the adsorbed acid phosphate regardless of the nature of initially precipitating mineral phase(s).

The similarity of *in vivo* and *in vitro* crystal growth events supports the concept that the precipitation mechanisms and the nature and morphology of the formed crystals are primarily determined by the driving force in the mineralizing milieu. It is most likely that the driving force for enamel mineralization is highest in the narrow region adjacent to the secretory ameloblasts, which tightly control Ca transport into the mineralizing milieu [25, 26]. Indeed, our previous studies on the enamel fluid surrounding the secretory enamel crystals [27, 28] showed that the separated enamel fluid was undersaturated with respect to OCP but may become supersaturated with respect to this salt by an increase in the Ca concentration up to 1 mM. The assumed declining concentration gradient of Ca, or the decreasing driving force, from the surface toward the inside of the secretory enamel is consistent with the observed transition in precipitation mechanisms from the initial precipitation of OCP-like thin ribbons, through the epitaxy and rapid overgrowth of apatites on the thin-ribbon template, to the thickening of apatite crystals at slow rates.

On the basis of the foregoing results and consideration, the crystal growth process taking place at early stages of porcine enamel mineralization is illustrated in Figure 5. (1) The two-dimensional growth of an OCP-like precursor occurs rapidly to yield thin-ribbon morphology elongating in length and width in a narrow outermost zone adjacent to the ameloblasts. (2) With the decrease of the driving force after precursor precipitation, the epitaxial growth of apatite on the thin ribbon is prominent in the underlying outer secretory enamel. (3) The lateral growth of isolated apatite units on the template leads to fusions of neighboring units, consequently giving rise to the elongated hexagonal shape. (4) Once enamel apatite crystals have flattened hexagonal shapes, their thickening continues at slow rates by acquisition of apatite unit cells on the prism planes of apatite crystals.

According to the proposed crystal growth model, it is germane to consider that the observed uniformity of enamel apatites with respect to their thickness is acquired by controlling the number of epitaxial sites on the thin ribbon and the growth rate of apatite nuclei. Nelson and Barry [29] postulated the presence of screw dislocations which emanate from the central planar defect because of slight OCP/apatite lattice mismatch there. Recently, Cuisinier et al. [30] demonstrated the presence of screw dislocations in young thin-plate crystallites of human fetal enamel. From our observations, it appears that the regular triangle images of the epitaxially formed apatite represent the continuous growth around screw dislocations. Intriguingly, those triangle images were replaced by the trapezoids. This phenomenon indicates that the growth rate in the horizontal direction was much faster than that in the vertical direction, leaving a broad lateral plane. A plausible explanation for this anisotropic growth reaction is that the screw dislocations may be extinguished with the deposition of carbonated apatite lamella or blocked by impurities. Under such circumstances, it is perceived that (1) the growth in the horizontal direction was able to advance rapidly by incorporation of the lattice units into remaining kink sites, which provide two-

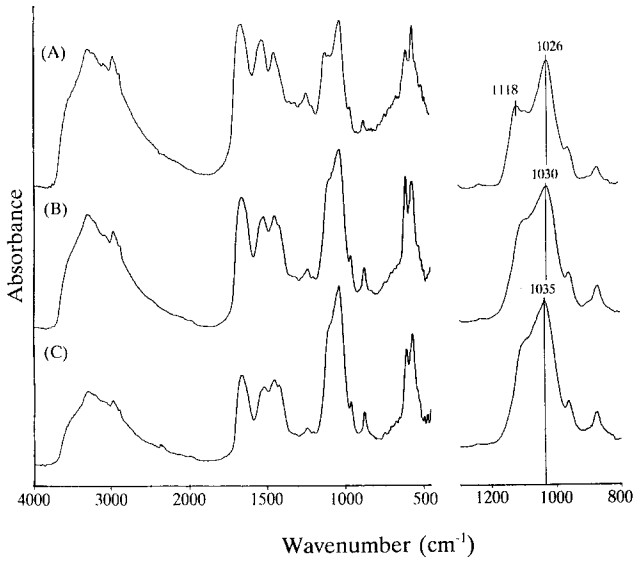

Fig. 4. FTIR experimental spectra of porcine enamel samples in the range of 4000 and 450 cm^{-1} (left) and their difference spectra in the range of 1300 and 800 cm^{-1} (right). **(A)** Outermost secretory enamel (less than 30 μm thick). **(B)** Outer secretory enamel dissected from the zone ranging from about 30 to 60 μm in depth from the enamel surface. **(C)** Underlying inner secretory enamel. Note the marked spectral changes with developmental advancement or mineralization, namely, the disappearance of the PO_4 band at 1118 cm^{-1} and a gradual shift of the peak maxima of PO_4 band from 1026 to 1035 cm^{-1}.

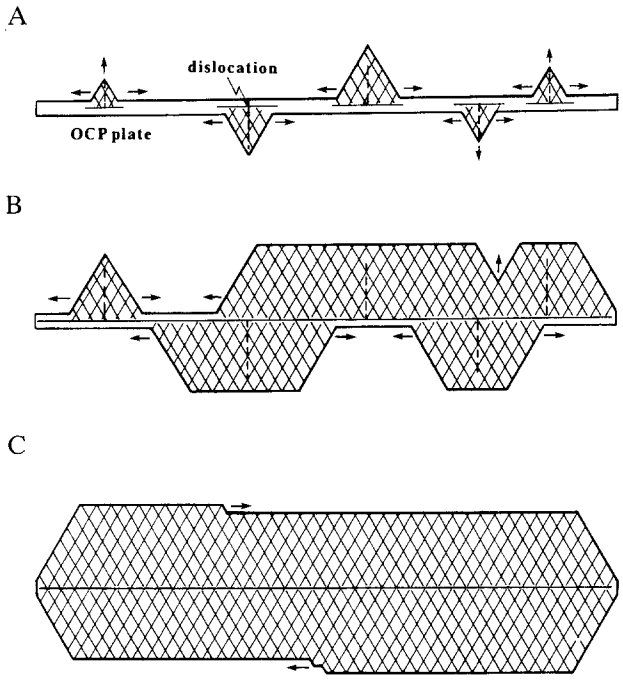

Fig. 5. Schematic illustration of enamel crystal growth occurring in early stages of porcine amelogenesis. **(A)** Epitaxial growth of apatite on the thin ribbon. **(B)** Lateral growth of isolated apatite units on the template and fusions of the neighboring units. **(C)** Thickening of apatite crystals by acquisition of apatite unit cells on their prism planes.

dimensionally both lateral and bottom supporting planes; in contrast (2) the growth in the vertical direction required acquisition of new apatite nuclei on the surface plane, which is energetically less stable. Similar consideration is relevant to the slow growth of enamel apatite crystals, mainly their thickening, after depletion of the kink sites by fusions of the trapezoids on the thin-ribbon precursors.

Another important conclusion from the proposed growth model is that the central dark line represents the vestige of the platy precursor, which was buried by the overgrowth of apatitic units. In connection with the embedding of the initial precursor, it is interesting to point out that the central dark line was found ubiquitously in most enamel crystallites, whereas its occurrence was much less frequent in synthetic carbonatoapatites and, as reported previously [24], in fish enameloid crystals containing high fluoride. Under conditions where OCP hydrolysis occurs rapidly (e.g., in the absence of proteinaceous inhibitors *in vitro* or by fluoride), the precursor structure may be converted into apatite before it is buried by the overgrown apatitic lamella. Our recent *in vitro* studies showed that platy OCP crystals were formed, but rapidly hydrolyzed in media containing low concentrations of fluoride (e.g., 0.05 ppm as found in the enamel fluid) [31]. It was also verified that the secreted enamel matrix proteins, particularly amelogenins, have adsorption affinity onto OCP crystals [16] and that the adsorbed proteins, in concert with carbonate and magnesium ions in the mineralizing milieu, stabilize the precursor phase (unpublished data).

In conclusion, the present studies indicate that the initial enamel mineralization comprises two events: the initial precipitation of OCP-like thin ribbons and the subsequent epitaxial growth of apatite crystals on the surfaces of the precursor. These precipitation reactions and the resulting morphological features are reproducible *in vitro*. The overall results support the importance of physicochemical mechanisms in determining the nature and properties of enamel mineral. It should be noted that the foregoing conclusion does not exclude the functional importance of matrix proteins in the initial stage of enamel mineralization. As mentioned briefly in relation to stabilization of the precursor phase, the abundance of proteinaceous crystal growth inhibitors in the outermost secretory enamel [32] contributes significantly to each of the initial mineralization steps. Their putative roles are to control the number and orientation of thin ribbons precipitated in the outermost region, to prevent random proliferation of apatite crystals, and to regulate the kinetics of apatite overgrowth on the precursor template. At present, most of their functional roles still remain speculative. More experimentation both *in vivo* and *in vitro* is required to gain a better insight into the protein-crystal interaction in the early stage of amelogenesis.

Acknowledgment. This work was supported by Grants DE07623 and DE08670 from the National Institute of Dental Research.

References

1. Nylen MU, Eanes ED, Omnell KA (1963) Crystal growth in rat enamel. J Cell Biol 18:109–123
2. Kerebel B, Daculsi G, Kerebel LM (1979) Ultrastructural studies of enamel crystallites. J Dent Res 58B:884–850
3. Weiss MP, Voegel JC, Frank RM (1981) Enamel crystallite growth: width and thickness study related to the possible presence of octacalcium phosphate during amelogenesis. J Ultrastruct Res 76:286–292

4. Brown WE, Schroeder LW, Ferris JS (1979) Interlayering of crystalline octacalcium phosphate and hydroxylapatite. J Phys Chem 83:1385–1388
5. Terpstra RA, Bennema P (1987) Crystal morphology of octacalcium phosphate: theory and observation. J Crystal Growth 82: 416–426
6. Nelson DGA, Salimi H, Nancollas GH (1986) Octacalcium phosphate and apatite overgrowths: a crystallographic and kinetic study. J Colloid Interface Sci 110:32–39
7. Iijima M, Tohda H, Moriwaki Y (1992) Growth and structure of lamellar mixed crystals of octacalcium phosphate and apatite in a model system of enamel formation. J Crystal Growth 116:319–326
8. Iijima M, Tohda H, Suzuki H, Yanagisawa T, Moriwaki Y (1992) Effects of F^- on apatite-octacalcium phosphate intergrowth and crystal morphology in a model system of tooth enamel formation. Calcif Tissue Int 50:357–361
9. Aoba T, Tanabe T, Moreno EC (1987) Function of amelogenins in porcine enamel mineralization during the secretory stage of amelogenesis. Adv Dent Res 1:252–260
10. Aoba T, Moreno EC (1990) Changes in the nature and composition of enamel mineral during porcine amelogenesis. Calcif Tissue Int 47:356–364
11. McKee MD, Aoba T, Moreno EC (1991) Morphology of the enamel organ in the miniature swine. Anat Rec 230:97–113
12. Shimoda S, Aoba T, Moreno EC (1991) Changes in acid phosphate content in enamel mineral during porcine amelogenesis. J Dent Res 70:1516–1523
13. Shimoda S, Aoba T, Moreno EC, Miake Y (1990) Effect of solution composition on morphological and structural features of carbonated calcium apatites. J Dent Res 69:1731–1740
14. Gee A, Deitz VR (1953) Determination of phosphate by differential spectrophotometry. Anal Chem 25:1320–1324
15. Conway EJ (1962): Microdiffusion analysis and volumetric error (5th ed). Crosby Lockwood & Son LTD, London, pp 201–214
16. Aoba T, Fukae M, Tanabe T, Shimizu M, Moreno EC (1987) Selective adsorption of porcine amelogenins onto hydroxyapatite and their inhibitory activity on seeded crystal growth of hydroxyapatite. Calcif Tissue Int 41:281–289
17. Daculsi G, Menanteau J, Kerebel LM, Mitre D (1984) Length and shape of enamel crystals. Calcif Tissue Int 36:550–555
18. Hohling HJ, Althoff J, Barckhaus R, Krefting ER, Lissner G, Quint P (1981) Early stages of crystal nucleation in hard tissues. In: Schweiger HG (ed) International cell biology, 1980–1981. Springer-Verlag, New York, pp 974–982
19. Nelson DGA, Wood GJ, Barry JC (1986) The structure of (100) defects in carbonated apatite crystallites: a high resolution electron microscope study. Ultramicroscopy 19:253–266
20. Siew C, Gruninger SE, Chow LC, Brown WE (1992) Procedure for the study of acidic calcium phosphate precursor phases in enamel mineral formation. Calcif Tissue Int 50:144–148
21. Rey C, Collins B, Goehl T, Shimizu M, Glimcher MJ (1991) Resolution-enhanced Fourier transformed infrared spectroscopy study of the environment of phosphate ions in the early deposits of a solid phase of calcium-phosphate in bone and enamel, and their evolution with age II: investigations in the mu_3 PO_4 domain. Calcif Tissue Int 49:383–388
22. Sauer GR, Wuthier RE (1988) Fourier transform infrared characterization of mineral phases formed during induction of mineralization by collagenase-released matrix vesicles in vitro. J Biol Chem 263:13718–13718
23. Pleshko N, Boskey A, Mendelsohn R (1991) Novel infrared spectroscopic method for the determination of crystallinity of hydroxyapatite minerals. Biophys J 60:786–793
24. Miake Y, Aoba T, Moreno EC, Shimoda S, Prostak K, Suga S (1990) Ultrastructural studies on crystal growth of enameloid minerals in elasmobranch and teleost fishes. Calcif Tissue Int 48:204–217
25. Bawden JW (1989) Calcium transport during mineralization. Anat Rec 224:226–233
26. Kawamoto T, Shimizu M (1990) Changes in the mode of calcium and phosphate transport during rate incisal enamel formation. Calcif Tissue Int 46:406–414
27. Aoba T, Moreno EC (1987) The enamel fluid in the early secretory stage of porcine amelogenesis. Chemical composition and saturation with respect to enamel mineral. Calcif Tissue Int 41: 86–94
28. Moreno EC, Aoba T (1987) Calcium binding in enamel fluid and driving force for enamel mineralization in the secretory stage of amelogenesis. Adv Dent Res 1:245–251
29. Nelson DGA, Barry JC (1989) High resolution electron microscopy of nonstoichiometric apatite crystals. Anat Rec 224:265–276
30. Cuisinier FJG, Steuer P, Frank RM, Voegel JC (1990) High resolution electron microscopy of young apatite crystals in human fetal enamel. J Biol Buccale 18:149–154
31. Mura-Galelli MJ, Narusawa H, Shimada T, Iijima M, Aoba T (1992) Effect of fluoride on precipitation and hydrolysis of octacalcium phosphate in an experimental model simulating enamel mineralization during amelogenesis. Cells Materials 2: 221–230
32. Tanabe T, Aoba T, Moreno EC, Fukae M, Shimizu M (1990) Properties of phosphorylated 32 kd non-amelogenin proteins isolated from porcine secretory enamel. Calcif Tissue Int 46: 205–215